

# The “Same Side – Opposite Side Effect” of the Heliospheric Current Sheet in Ionospheric Negative Storms

Z. Li · F.S. Wei · X.S. Feng · X.H. Zhao

Received: 3 October 2009 / Accepted: 4 April 2010 / Published online: 24 April 2010  
© Springer Science+Business Media B.V. 2010

**Abstract** Using 141 CME-interplanetary shock (CME-IPS) events and foF2 from eight ionosonde stations from January 2000 to September 2005, from the statistical results we find that there is a “same side – opposite side effect” in ionospheric negative storms, *i.e.*, a large portion of ionospheric negative disturbances are induced by the same-side events (referring to the CMEs whose source located on the same side of the heliospheric current sheet (HCS) as the Earth), while only a small portion is associated with the opposite-side events (the CMEs source located on the opposite side of the HCS as the Earth); the ratio is 128 vs. 46, and it reaches 41 vs. 14 for the intense ionospheric negative storms. In addition, the ionospheric negative storms associated with the same-side events are often more intense. A comparison of the same-side event (4 April 2000) and the opposite-side event (2 April 2001) shows that the intensity of the ionospheric negative storm caused by the same-side event is higher than that by the opposite-side event, although their initial conditions are quite similar. Our preliminary results show that the HCS has an “impeding” effect to CME-IPS, which results in a shortage of energy injection in the auroral zone and restraining the development of ionospheric negative perturbations.

**Keywords** CME-interplanetary shock (CME-IPS) events · Heliospheric current sheet (HCS) · Ionospheric storms

## 1. Introduction

The heliospheric current sheet (HCS), frozen in the solar wind and spread to the interplanetary space, is the boundary encircling the Sun that separates oppositely directed magnetic fields originating from the Sun, and it also represents the magnetic equator of the global

---

Z. Li (✉) · F.S. Wei · X.S. Feng · X.H. Zhao  
SIGMA Weather Group, State Key Laboratory of Space Weather, Center for Space Science and Applied Research, Chinese Academy of Sciences, P.O. Box 8701, Beijing 100190, China  
e-mail: [zli@spaceweather.ac.cn](mailto:zli@spaceweather.ac.cn)

Z. Li  
Graduate University of the Chinese Academy of Sciences, Beijing, China

heliosphere (Ness and Wilcox, 1964; Wilcox and Ness, 1965; Smith, 2001). Since the HCS is a characteristic reference surface for the organization of the solar wind plasma, the influence of the HCS on the propagation and geoeffectiveness of solar disturbances in the interplanetary space have been studied in many papers (Burlaga, Hundhausen, and Zhao, 1981; Wei, Zhang, and Huang, 1990; Wei, Liu, and Zhang, 1991; Wei and Dryer, 1991; Zhao and Feng, 2005).

Ionospheric storms usually refer to intense changes of the total electron content (TEC) of the ionosphere and ionospheric critical frequency ( $f_{\text{OF2}}$ ), which persist from several hours to days and are associated with magnetic disturbances (see, e.g., Prölss, 1995; Fuller-Rowell *et al.*, 1996; Maruyama, Ma, and Nakamura, 2004). Ionospheric storms are often described as positive storms when  $f_{\text{OF2}}$  is increased and as negative storms when  $f_{\text{OF2}}$  is significantly reduced. The negative storm is caused by changes in the atmospheric composition, and this explanation has been fully supported by analyzer measurements (Prölss, 1980). At the main phase of a magnetic storm, the enhanced energy input from the magnetosphere causes considerable heating of the ionized and neutral gases in the auroral zone, leading to the “composition bulges”. They are characterized by enhanced  $[N_2]/[O]$  and they propagate to lower latitudes carried by the horizontal neutral winds that arise from the pressure gradient force in the auroral oval and by ion drag in the polar cap. Then they cause negative storms by increasing the loss rate and decreasing the ionospheric electron density (see, e.g., Prölss, 1981, 1993; Buonsanto, 1999; Burns, Killeen, and Roble, 1991; Fuller-Rowell, Codrescu, and Araujo-Pradere, 2001).

Feng and Zhao (2006) and Xie *et al.* (2006) investigated the effect of HCS on propagation and geoeffectiveness of CME-ICME events and CME-IP shock events, respectively. In their work, the geoeffectiveness is limited as regards the geomagnetic activity. In this paper, we choose 141 CME-IPS events from January 2000 to September 2005 and study the influence of the HCS on the geoeffectiveness of these events, especially on the response of the ionosphere, by statistics and by a case study.

## 2. Data Used for the Study

We select 141 IP shocks that occurred from January 2000 to September 2005 from a list of CME-associated shocks, which is compiled using events reported in the literature (McKenna-Lawlor *et al.*, 2002; Cane and Richardson, 2003; Cho *et al.*, 2003; Fry *et al.*, 2003; Manoharan *et al.*, 2004; Schwenn *et al.*, 2005), supplemented with the shock list obtained from the proton monitor (PM) instrument on board the SOHO mission (available at <http://umtof.umd.edu/pm/FIGS.HTML> and <http://www.gi.alaska.edu/pipermail/gse-ff>). As for each event, we draw the solar magnetic field synoptic chart of the Carrington rotation during which the CME erupted according to the observations of the Wilcox Solar Observatory (<http://quake.stanford.edu/~wso/coronal.html>). The magnetic field data and the proton data are obtained from MFI and SWE instruments on board the Wind spacecraft. Besides, the geomagnetic activity indices,  $D_{\text{st}}$ ,  $AE$  and  $K_p$ , are obtained from the World Data Center for Geomagnetism, Kyoto (<http://swdcwww.kugi.kyoto-u.ac.jp/index.html>).

The values of  $f_{\text{OF2}}$  of eight ionosonde stations (Eglin AFB, Goosebay, Learmonth, Manzhouli, Millstone Hill, Mundaring, Port Stanley, Wallops Is.) during 2000–2005 are obtained from the SPIDR (Space Physics Interactive Data Resource) network of the National Geophysical Data Center. In our investigations,  $D(f_{\text{OF2}})$  is used to describe the response of the F2 region to geomagnetic storms; that is, the relative deviations of the critical frequency

from the quiet level:

$$D(\text{foF2}) = \frac{\text{foF2} - (\text{foF2})_{\text{med}}}{(\text{foF2})_{\text{med}}}.$$

Here  $\text{foF2}$  is the hourly value of perturbed critical frequency and  $(\text{foF2})_{\text{med}}$  represents the monthly median of  $\text{foF2}$ . In our study, we consider an ionospheric disturbance as a negative storm when  $D(\text{foF2})$  is less than  $-0.15$  and the negative disturbances persist over 6 hours. We will use  $D(\text{foF2})_{\text{min}}$ , which is the minimum value of  $D(\text{foF2})$  for our following statistics.

### 3. Statistics of Ionospheric Responses to the Same-Side and Opposite-Side Events

We first classify these 141 CME-IPS events into categories according to the relative positions of the solar source and the Earth with respect to the HCS at the solar source surface: *i*) same-side events, for which the solar source and the sub-Earth point are located on the same side of the HCS when the CME occurred; *ii*) opposite-side events, for which the solar source and the sub-Earth point are located on the opposite sides of the HCS at the time of CME's initiation.

Figure 1 displays the distributions of the ionospheric negative storm intensity against the angular distance between the Earth and the HCS (top) and against the magnetic storm intensity (bottom). Asymmetric distributions can be seen in this figure. On the one hand, in these 141 CME-IP events, the angular distances between the Earth and the HCS of the same-side events may reach  $58^\circ$ , while the angular distances of the opposite-side events do not exceed  $40^\circ$ . On the other hand, magnetic storms and ionospheric negative storms have positive correlation to a certain extent, and intense ionospheric negative storms are usually associated with intense magnetic storms. Furthermore, the distributions are obviously asymmetric: the event frequency of the same-side events is distinctly higher than that of the opposite-side events, and the majority of intense magnetic storms and ionospheric negative storms are induced by the same-side events.

There are 66 cases in the 141 CME-IPS events that caused geomagnetic storms and 174 ionospheric negative storms in the eight ionosonde stations. In order to investigate whether the statistical distributions of ionospheric negative storms are affected by the same side–opposite side effect, we classify 174 cases into three levels according to the value of  $D(\text{foF2})_{\text{min}}$ , and then consider the classification of the same-side and the opposite-side events. The results are shown in Figure 2a: *i*) level a ( $-0.3 \leq D(\text{foF2})_{\text{min}} < -0.15$ ) includes 17 cases, and 14 of them are induced by the same-side events, while only 3 cases are induced by the opposite-side events; *ii*) level b ( $-0.5 \leq D(\text{foF2})_{\text{min}} < -0.3$ ) includes 102 cases, and 73 of them are the same-side events, while 29 of them are opposite-side events; *iii*) level c ( $D(\text{foF2})_{\text{min}} < -0.5$ ) includes 55 cases, and 41 of them are induced by the same-side events, while 14 of them are associated with the opposite-side events. There are 174 ionospheric negative storms in total; the ratio of the number of ionospheric negative storms triggered by the same-side events to that of storms triggered by the opposite-side events is  $128/46 \approx 2.78$ .

As a comparison study, the statistics of the 66 magnetic storms are shown in Figure 2b. We can see that the numbers of weak magnetic storms ( $-50 \text{ nT} \leq D_{\text{stmin}} < -30 \text{ nT}$ ) associated with the same-side events and the opposite-side events are 9 and 6, respectively; for moderate magnetic storms ( $-100 \text{ nT} \leq D_{\text{stmin}} < -50 \text{ nT}$ ), the numbers are 17 and 5, respectively; and for intense magnetic storms ( $D_{\text{stmin}} < -100 \text{ nT}$ ), the numbers are 22 and 7,

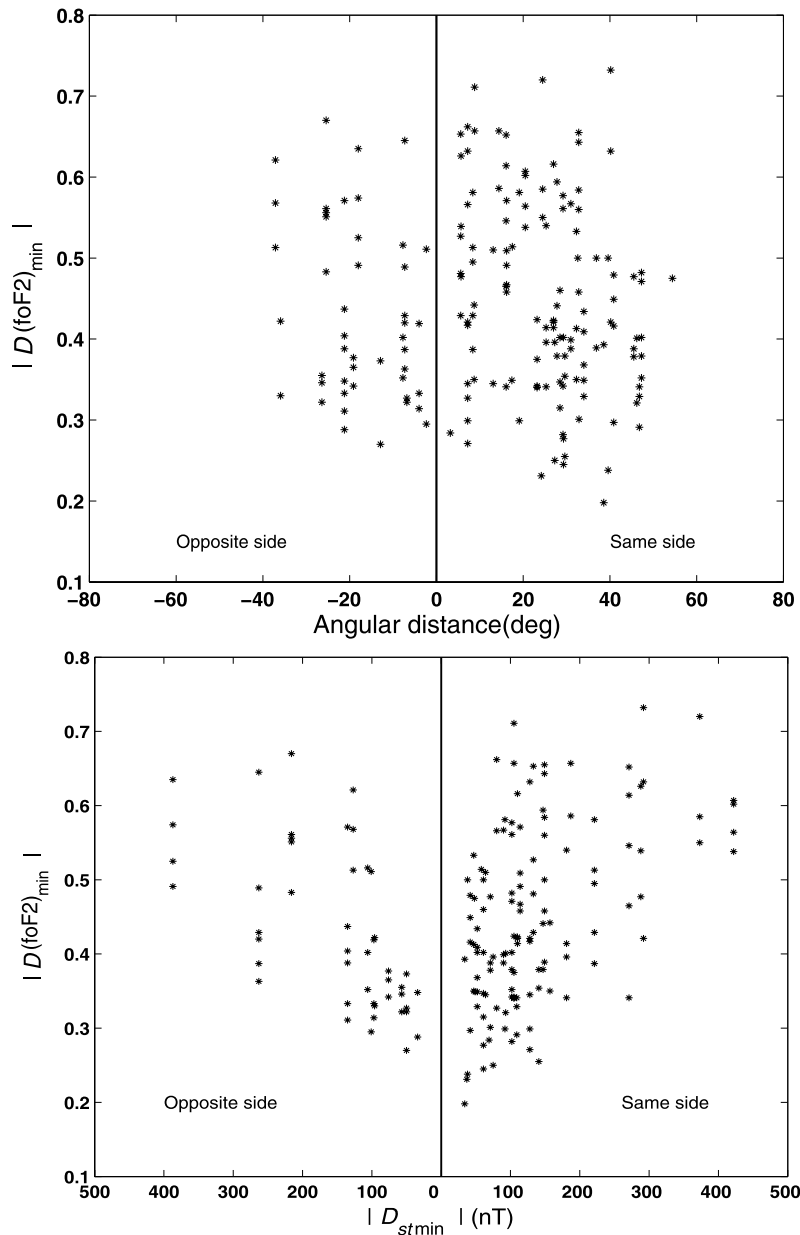


**Figure 1** Distributions of the ionospheric negative storm intensity with respect to the angular distance between the Earth and the HCS (top) and to the magnetic storm intensity (bottom).

respectively. To sum up, there are 48 magnetic storms caused by the same-side events, while only 18 magnetic storms resulted from the opposite-side events; the ratio is  $48/18 \approx 2.67$ .

The above results indicate that there is a “same side – opposite side effect” in the geomagnetic storms and ionospheric negative disturbances: in our statistics, the geomagnetic

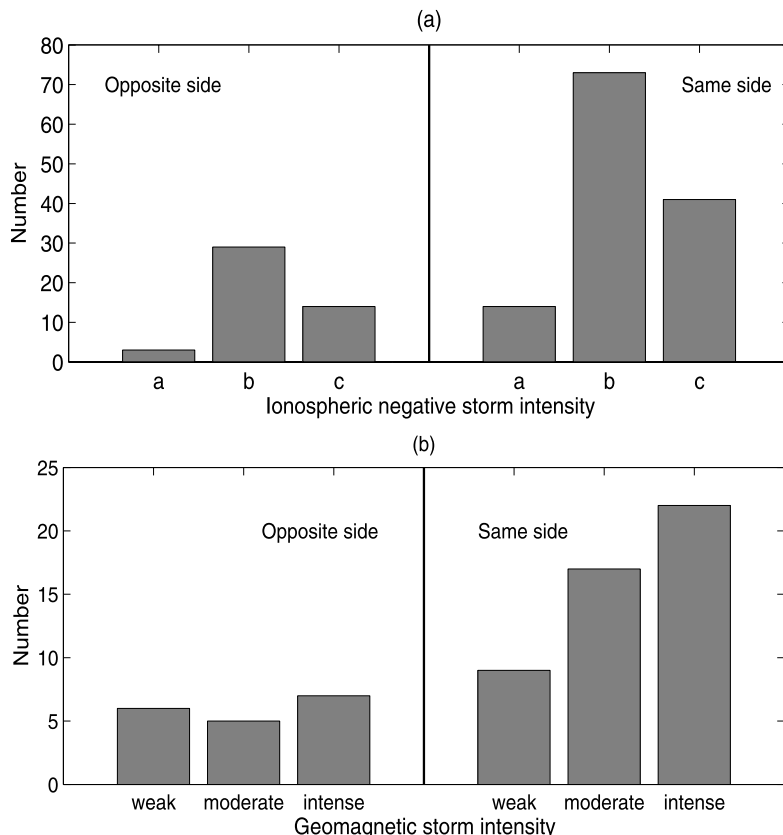
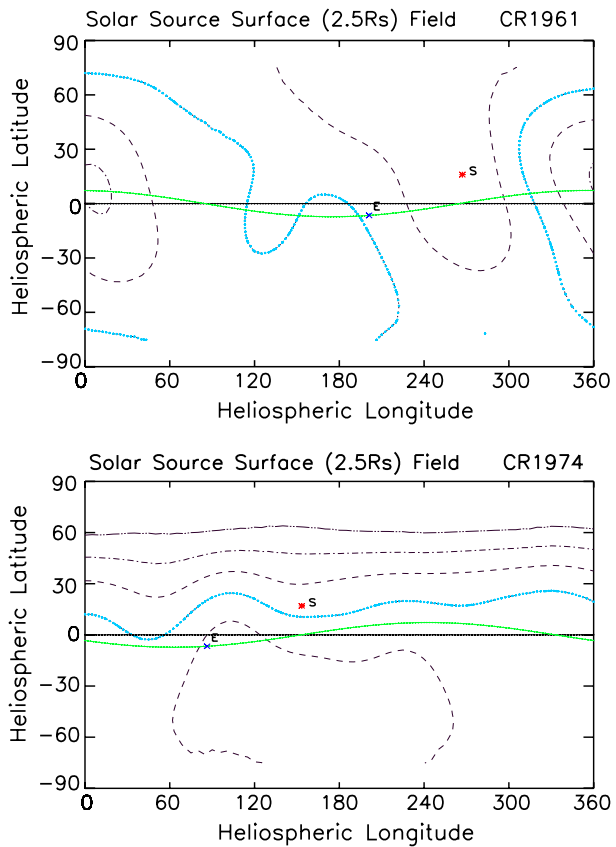


**Figure 2** The same side–opposite side effect in terms of the distributions of (a)  $D(\text{foF}2)_{\min}$  and (b) geomagnetic storm intensity. In panel (a), levels a, b, and c represent  $-0.3 \leq D(\text{foF}2)_{\min} < -0.15$ ,  $-0.5 \leq D(\text{foF}2)_{\min} < -0.3$ , and  $D(\text{foF}2)_{\min} < -0.5$ , respectively.

storms and ionospheric storms are mainly associated with the same-side events. Especially, on every level of magnetic storms and ionospheric negative storms, the number of the same-side events is higher than that of the opposite-side events. Furthermore, there is a tendency that the ionospheric negative storms associated with the same-side events are often a bit more intense than those induced by the opposite-side events. Hence, the HCS is an important reference surface for investigating the chain of “CME-IPS–geomagnetic disturbances–ionospheric negative disturbances”. However, it should be noted that besides the same side–opposite side effect many other key factors must also be considered, such as the angular distance between the solar source and the HCS, IMF  $B_z$  and the quite different situations near the terrestrial space for each event. Though there is a close relationship between magnetic storms and ionospheric disturbances, from Figure 2 we can see that their distributions are not quite similar. That is because the levels of intensity of the ionospheric negative storms do not correspond to the levels of intensity of the magnetic storms absolutely, and the ionospheric perturbations are very complicated processes and also are affected by many other factors such as local time, latitude and season.

**Figure 3** The spread of CME source on solar magnetic field synoptic chart (the projections of the CME's source location and the Earth are marked by S and E respectively, and the blue thick dotted lines represent the HCS, the green thin solid lines represent the ecliptic plane, the broken lines represent the isograms of solar magnetic field). (Top) The same-side event (associated CME on 4 April 2000 16:32 UT at N16W66); (bottom) the opposite-side event (associated CME on 2 April 2001 22:06 UT at N17W67).

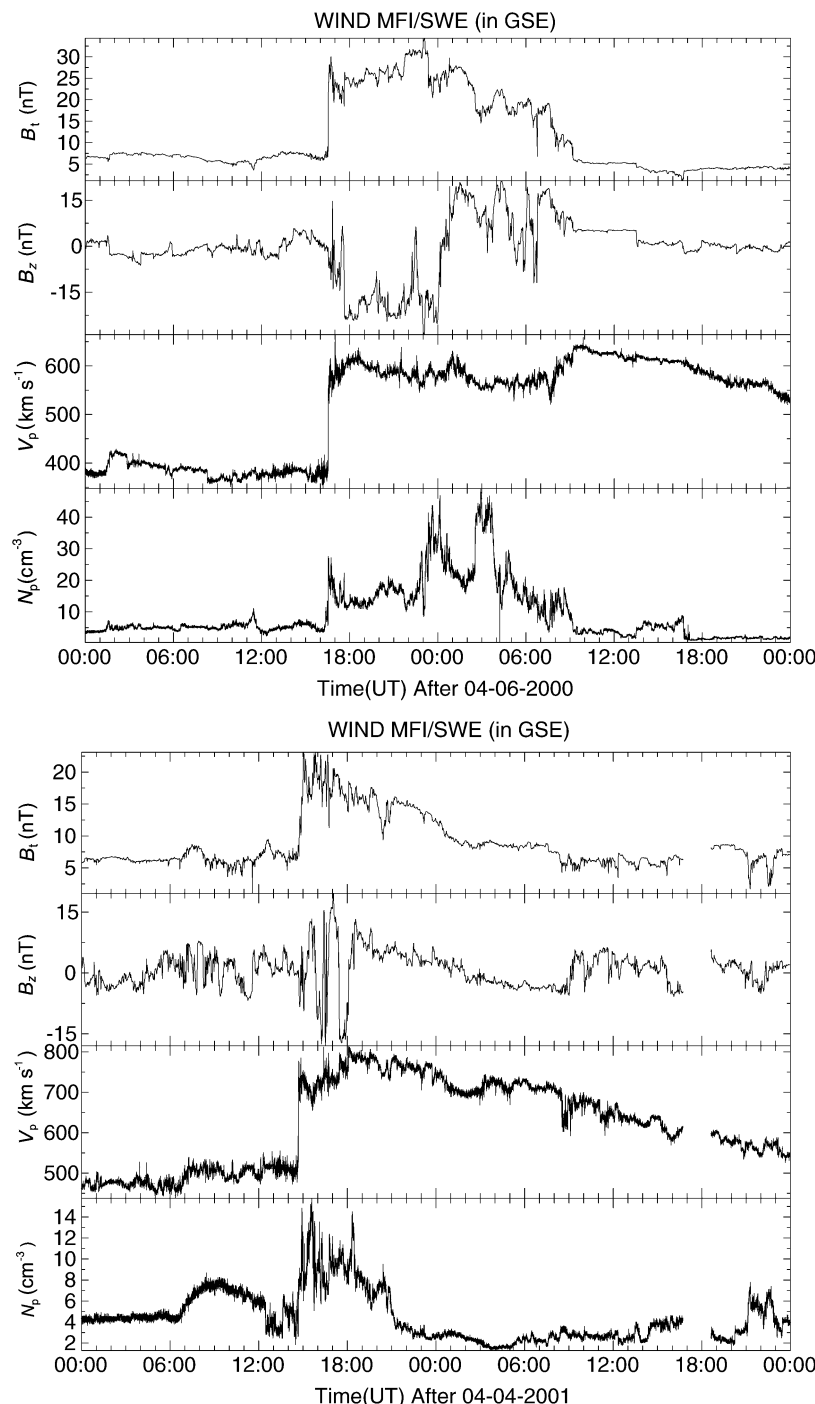


#### 4. Case Study

In this section, we select two cases for our comparison study: one is a same-side event and the other is an opposite-side event. The synoptic charts of the solar magnetic field of the two cases are shown in Figure 3. The blue thick dotted lines represent the HCS, the thin green solid lines represent the ecliptic plane, the broken lines represent the isograms of solar magnetic field, “S” represents the source location of CME, while “E” is the sub-Earth point at CME erupting time. These two cases have similar initial conditions: *i*) the same-side event (top panel): the time of the CME eruption is at 16:32 UT on 4 April 2000, the solar source coordinates are at N16W66 and the initial speed of the shock is about  $2000 \text{ km s}^{-1}$ ; *ii*) the opposite-side event (bottom panel): the time of the CME eruption is at 22:06 UT on 2 April 2001, the solar source coordinates are at N17W67, the initial speed of the shock is about  $2300 \text{ km s}^{-1}$ . So we can compare the geomagnetic and ionospheric disturbances of these two cases in order to emphasize and investigate the influence of the HCS on the geoeffectiveness of CME-IPS.

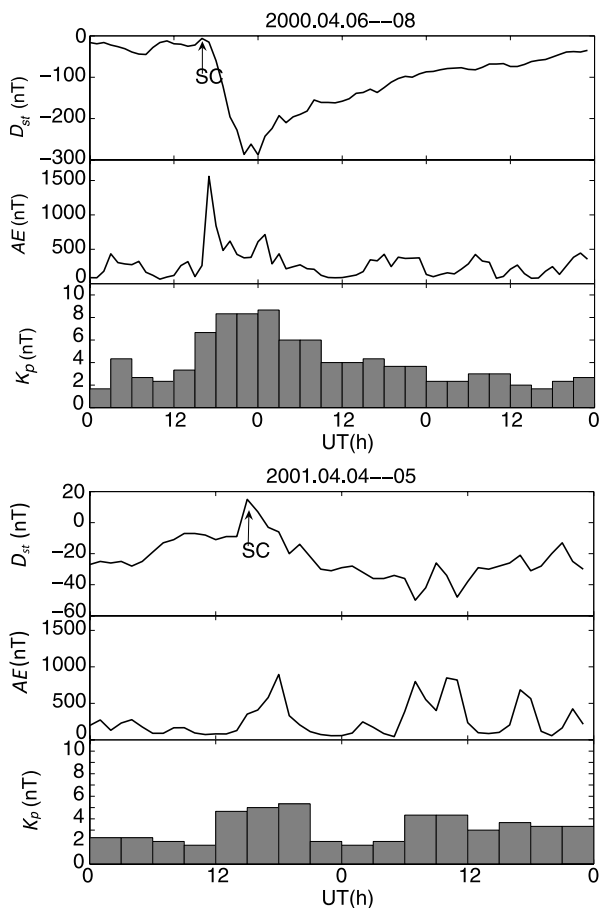
##### 4.1. The Comparison of the Interplanetary Disturbances and the Geomagnetic Disturbances

Figure 4 shows the interplanetary conditions – the IMF  $B_t$ , IMF  $B_z$ , the proton velocity  $V_p$  and the proton number density  $N_p$  from the Wind spacecraft during the period from (top)



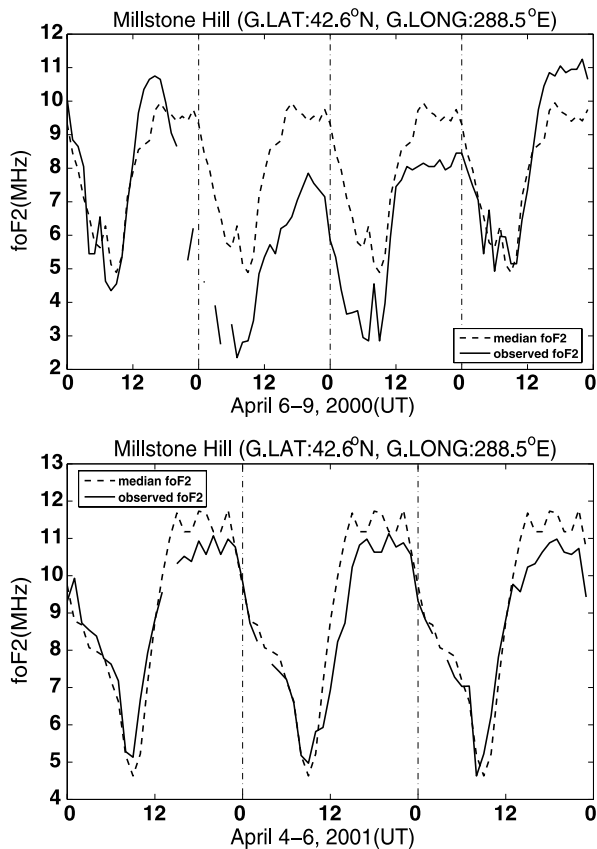
**Figure 4** Interplanetary conditions in the periods of 6–7 April 2000 (top) and 4–5 April 2001 (bottom).

**Figure 5** Geomagnetic indices in the periods of 6–8 April 2000 (top) and 4–5 April 2001 (bottom).



6 to 7, April 2000 and (bottom) 4 to 5, April 2001, respectively. It is notable that the IMF  $B_z$  turned southward abruptly at about 17:40 UT on 6 April 2000 and stayed negative for more than 6 hours for the same-side event, as shown in the top panel of Figure 4. On the other hand, for the opposite-side event, as shown in the bottom panel of Figure 4, the IMF  $B_z$  oscillated between northward and southward during 16:00–18:00 UT on 4 April 2001 and did not have a long-lasting southward component during the period of the case. The geomagnetic indices  $D_{st}$ ,  $AE$  and  $K_p$  in the periods of 6–8 April 2000 (top) and 4–5 April 2001 (bottom) are shown in Figure 5, respectively. For the same-side event, as shown in the top panel of Figure 5, the onset of an intense magnetic storm was at about 17:30 UT on 6 April, and the magnetic field started to decrease monotonically, with a rate of change of  $-54.4 \text{ nT h}^{-1}$  for 18:00–23:00 UT. It reached its maximum depression of  $-288 \text{ nT}$  at 01:00 UT on 7 April. After the maximum depression,  $D_{st}$  turned to the recovery phase and went back to the quiet level gradually in the midnight on 8 April. For the opposite-side event, as the bottom panel of Figure 5 shows,  $D_{st}$  reached its maximum depression of  $-50 \text{ nT}$  at 08:00 UT on 5 April, the rate of change is  $-4.1 \text{ nT h}^{-1}$  for 16:00 UT on 4 April to 08:00 UT on 5 April, and  $D_{st}$  was back at the quiet level after 18:00 UT on 5 April.

**Figure 6** Solid lines are foF2 in the periods of 6–9 April 2000 (top) and 4–6 April 2001 (bottom). Broken lines represent reference foF2, which are the medians of April 2000 (top) and April 2001 (bottom).



From the discussions above, it is obvious that the same-side event had greater interplanetary disturbances, more intense and longer lasting negative IMF  $B_z$ , and then caused an intense magnetic storm, while the opposite-side event caused a weak magnetic storm.

#### 4.2. The Comparison of the Ionospheric Disturbances

In this section, foF2 of Millstone Hill will be used as an example. The behavior of foF2 (the solid lines) in the periods of 6–9 April 2000 (top) and 4–6 April 2001 (bottom) are given in Figure 6. The broken lines are taken as a reference, which represent the median foF2 for that month. For the same-side event, as the top panel of Figure 6 shows, responding to the magnetic storm, foF2 started to decrease at 18:30 UT and turned to negative at 19:30 UT on 6 April. The maximum depression was  $-4.16$  MHz at 23:00 UT on 6 April and  $D(\text{foF2})_{\min} = -0.63$  was at 07:00 UT on 7 April. The negative disturbances persisted until the sunset on 8 April. For the opposite-side event, as the bottom panel of Figure 6 shows, over the three days after the occurrence of the magnetic storm, the negative disturbances were small and only occurred in the daytime of the local time (5 UT); the maximum depression was  $-1.45$  MHz at 14:00 UT on 6 April. Since  $D(\text{foF2})_{\min}$  is not less than  $-0.15$  and the disturbances did not persist over 6 hours for the opposite-side event, we consider it as a negative disturbance but not a negative storm.

Summing up, the ionospheric disturbances associated with the same-side event are more intense and last from daytime to nighttime of the local time. To compare, the opposite-side event induced weak ionospheric negative disturbances, which only occurred in the daytime of the local time.

The same-side event and the opposite-side event have similar initial conditions, but from the comparison and discussions above, their geoeffectivenesses are significantly different: the same-side event had greater interplanetary disturbances and caused an intense geomagnetic storm, with a great energy input to the auroral zone, the “composition bulges” propagated to lower latitudes carried by equatorward neutral winds, and then caused a negative storm by increasing the loss rate and decreasing the ionospheric electron density. On the other hand, the interplanetary, geomagnetic, and ionospheric disturbances associated with the opposite-side event are relatively weak. Hence, it is suggested that the opposite-side event does not induce intense geomagnetic and ionospheric disturbances easily because of the “impeding” effect of HCS on the propagation of the CME-IPS.

## 5. Conclusions and Discussion

Based on the analysis of observational data, we investigate the geoeffectiveness, especially the response of the ionosphere to the 141 CME-IPS events using statistics and a case study, and the following conclusions are obtained.

i) The same-side events are more likely to induce geoeffectiveness, including geomagnetic and ionospheric disturbances. In our statistics, the rate of the number of geomagnetic disturbances associated with the same-side events to those induced by the opposite-side events is 2.67, while the rate of the number of ionospheric disturbances is 2.78.

ii) On every level of intensity of geomagnetic and ionospheric disturbances, the numbers of the same-side events is higher than that of the opposite-side events. Especially, the majority of intense geomagnetic and ionospheric disturbances are induced by the same-side events: the number of intense magnetic storms triggered by the same-side events and the opposite-side events are 22 and 7 respectively, while the numbers of intense ionospheric negative storms ( $D(\text{f}o\text{F}2)_{\min} < -0.5$ ) are 41 and 14, respectively.

iii) In our case study, the intensity and duration of negative IMF  $B_z$ , geomagnetic and ionospheric disturbances associated with the same-side event are more intense and longer than those induced by the opposite-side event in the case of the similar initial conditions, which include the solar source coordinates and the shock’s initial speed.

iv) The HCS has an “impeding” effect on the propagation of CME-IPS, which results in a shortage of energy injection in the auroral zone, and a shortage of energy injection restrains the development of ionospheric negative storms.

Hence, the HCS is an important reference surface for investigating the chain of “CME-IPS – geomagnetic disturbances – ionospheric negative disturbances”. These results are relevant in the field of space weather, especially in predicting geomagnetic and ionospheric disturbances. Thus, the physical process of the same side–opposite side effect upon ionospheric negative storms and how to establish a predicting model based on this are subjects worthy of further study.

**Acknowledgements** This work is jointly supported by the National Natural Science Foundation of China (40890162, 40704030 and 40674084) and the Specialized Research Fund for State Key Laboratories.

## References

- Buonsanto, M.J.: 1999, *Space Sci. Rev.* **88**, 563.
- Burlaga, L.F., Hundhausen, A.J., Zhao, X.P.: 1981, *J. Geophys. Res.* **86**, 8893.
- Burns, A.G., Killeen, T.L., Roble, R.G.: 1991, *J. Geophys. Res.* **96**, 14153.
- Cane, H.V., Richardson, I.G.: 2003, *Space Sci. Rev.* **88**, 563.
- Cho, K.-S., Moon, Y.-J., Dryer, M., Fry, C.D., Park, Y.-D., Kim, K.-S.: 2003, *Astrophys. Space Sci.* **108**, 1445.
- Feng, X.S., Zhao, X.H.: 2006, *J. Geophys. Res.* **105**, 37.
- Fry, C.D., Dryer, M., Deehr, C.S., Sun, W., Akasofu, S.-I., Smith, Z.: 2003, *J. Geophys. Res.* **108**, 1070.
- Fuller-Rowell, T.J., Codrescu, M.V., Rishbeth, H., Moffett, R.J., Quegan, S.: 1996, *J. Geophys. Res.* **101**, 2343.
- Fuller-Rowell, T.J., Codrescu, M.V., Araujo-Pradere, E.A.: 2001, In: Song, P., Singer, H.J., Siscoe, G.L. (eds.) *Space Weather; AGU Geophys. Monogr.* **125**, 393.
- Manoharan, P.K., Gopalswamy, N., Yashiro, S., Lara, A., Michalek, G., Howard, R.A.: 2004, *J. Geophys. Res.* **109**, A06109.
- Maruyama, T., Ma, G., Nakamura, M.: 2004, *J. Geophys. Res.* **109**, A10302.
- McKenna-Lawlor, S.M.P., Dryer, M., Smith, Z., Kecskemeti, K., Fry, C.D., Sun, W., Deehr, C.S., Berdichevsky, D., Kudela, K., Zastenker, G.: 2002, *Ann. Geophys.* **20**, 917.
- Ness, N.F., Wilcox, J.M.: 1964, *Phys. Rev. Lett.* **13**, 461.
- Prölss, G.W.: 1980, *Rev. Geophys. Space Phys.* **18**, 183.
- Prölss, G.W.: 1981, *J. Geophys. Res.* **86**, 2385.
- Prölss, G.W.: 1993, *Ann. Geophys.* **11**, 1.
- Prölss, G.W.: 1995, In: Volland, H. (ed.) *Handbook of Atmospheric Electrodynamics II*, CRC Press, Boca Raton, 195.
- Schwenn, R., Dal Lago, A., Huttunen, E., Gonzalez, W.D.: 2005, *Ann. Geophys.* **23**, 1033.
- Smith, E.J.: 2001, *J. Geophys. Res.* **106**, 15819.
- Wei, F.S., Dryer, M.: 1991, *Solar Phys.* **132**, 373.
- Wei, F.S., Zhang, J.H., Huang, S.P.: 1990, *Acta Geophys. Sin.* **33**, 125.
- Wei, F.S., Liu, S.Q., Zhang, J.H.: 1991, *Acta Geophys. Sin.* **34**, 133.
- Wilcox, J.M., Ness, N.F.: 1965, *J. Geophys. Res.* **70**, 5793.
- Xie, Y.Q., Wei, F.S., Xiang, C.Q., Feng, X.S.: 2006, *Solar Phys.* **238**, 377.
- Zhao, X.H., Feng, X.S.: 2005, *Sci. China E* **48**, 648.